Model-Predictive Sliding-Mode Control for Three-Phase AC/DC Converters

Tingting He, *Student Member, IEEE*, Dylan Dah-Chuan Lu, *Senior Member, IEEE*, Li Li, Jianwei Zhang, *Student Member, IEEE*, Linfeng Zheng, *Student Member, IEEE*, and Jianguo Zhu, *Senior Member, IEEE*

***Abstract*—This paper presents a model-predictive sliding-mode control (MPSMC) scheme for a three-phase ac/dc converter to achieve better stability and dynamic performances. In the conventional model-predictive control method, a proportional–integral (PI) controller is used to generate the active power reference. This traditional model-predictive PI control (MPPIC) scheme, however, produces a large overshoot/undershoot, a long settling time, and a large steady-state error under disturbances. To overcome these deficiencies, a sliding-mode controller is employed to replace the PI controller. Since the control law and the controller are designed based on the system model, the proposed MPSMC scheme can reduce the effects of unexpected disturbances, such as the output voltage demand and the resistance load variations. Both methods have been simulated in MATLAB/Simulink during various disturbances. Compared with the performances of MPPIC, the results obtained from MPSMC show that the settling time of the dc voltage can be minimized by about 91%, and the overshoot can be eliminated from 9.13% during the steady-state progress. The active and reactive power from MPSMC can also be controlled to the desired values, respectively, with a much smaller overshoot/undershoot and a faster response speed. Similar dynamic improvements can be achieved with MPSMC when the dc voltage demand varies. The simulation results are validated by experimental results.**

***Index Terms*—AC/DC converter, model-predictive control (MPC), proportional–integral (PI) controller sliding-model control.**

I. Introduction

THREE-PHASE switching ac/dc converters have recently attracted significant attentions because of their abilities to achieve bidirectional power flow, low harmonic line current, controllable power factor, and good dc-link voltage regulation [1]. They are the preferred converter topology in many industrial power systems [2] and have found extensive applications, such as railway electrification systems [3], renewable energy systems (wind power generation) [4], smart microgrids [5], and dc transmission systems [6]. Various advanced converter control strategies for three-phase ac/dc converters have been proposed [7], [8]. Remarkably stable and efficient schemes are employed to improve the power quality and reduce the effects caused by unexpected disturbances [9], [10]. Some good examples are voltage-oriented control (VOC), direct power control (DPC), and model-predictive control (MPC), which have been extensively and systematically studied.

Based on a converter system model in the rotational frame (*dq* coordinate), the classic VOC method applies the pulse width modulation (PWM) to control the active and reactive powers to track their references asymptotically [11]. Since most of the PWM methods ensure the harmonics on the output side, the converter input current ripple might be introduced, as well as the power ripples [12], [13]. A voltage outer loop and a current inner loop are also included in this scheme, and proportional–integral (PI) controllers are used in these two loops because of their simple structures. However, another drawback of this strategy is that the corresponding performances are highly dependent on the PI parameters and the current loop [14]. The stability and dynamic performance will be limited by the fixed PI parameters during disturbances. Controlling the active and reactive power through a switching table, the DPC scheme does not require the internal current control loop and PWM modulator block [15], [16]. Due to the difficulty in constructing a perfect heuristic table, the DPC method is also susceptible to producing large power ripples, which would affect the system steady-state performance [17].

Compared with the above two methods, the MPC method is a model-based control technique, which provides fast demand tracking speed and low-power ripples [18], [19], such as free of modulation, simple inclusion of system parameters, constraints, and demands in the algorithm [20]. For a two-level converter, MPC is devised to select an optimal switching state from eight possible states to obtain an optimal voltage vector. Based on the system model, a cost function is designed to minimize the errors between the references and the real-time acquisitions of the controlled variables. In a standard MPC strategy, a PI controller is used to generate the active power reference, which will be transferred to the cost function. The PI controller gains of this model-predictive PI control (MPPIC) scheme should be tuned and adjusted in an ad-hoc manner to satisfy the latest system demands and unknown disturbances. However, the PI parameters are constant and fixed during the operation. It is

Manuscript received June 4, 2017; revised July 27, 2017 and October 10, 2017; accepted December 6, 2017. Date of publication December 14, 2017; date of current version July 15, 2018. This work was supported by the China Scholarship Council (201407090060). Recommended for publication by Associate Editor M. Ordonez. *(Corresponding author: Tingting He.)*

The authors are with the School of Electrical and Data Engineering, The University of Technology Sydney, Sydney, NSW 2007, Australia (e-mail: Tingting.He@student.uts.edu.au; Dylan.Lu@uts.edu.au; Li.Li@uts.edu.au; jianwei.zhang-1@student.uts.edu.au; linfeng.zheng@student.uts.edu.au; jianguo.zhu@uts.edu.au).

Color versions of one or more of the figures in this paper are available online at http://ieeexplore.ieee.org.

Digital Object Identifier 10.1109/TPEL.2017.2783859

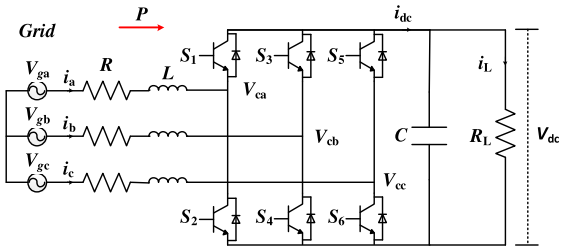

Fig. 1. Topology of a three-phase ac/dc converter.

hard for them to be tuned automatically according to the latest system objectives and the updated load demand.

In order to solve this problem, a sliding-mode control (SMC) scheme is considered to improve both the dynamic and steady-state performances. SMC is known for its excellent dynamic response and strong robustness to disturbances and uncertainties, such as unknown variations of control variables and system parameters [21]–[23]. As an effective nonlinear control technique, a control signal is employed to guide the system trajectory points onto a surface, known as the sliding surface or hyperplane. All the trajectory points will be forced to the vicinity of the sliding surface within a finite time and toward the system equilibrium point thereafter [24]. During the operation of unknown uncertainties, a control law is designed to maintain the control variables on the sliding surface [25]. In addition, SMC is simple to implement and execute.

This paper presents an MPC method incorporated with an SMC controller, known as the model-predictive sliding-mode control (MPSMC), to compensate the weakness of the standard MPC method using a PI controller. The SMC technique is employed to track the active power reference to improve the system dynamic performance and robustness. Since the system parameters are required in designing the controller and the controller law, system parameter identification plays a vital role in the SMC. When controlling a complex system, it might be difficult to get highly accurate system parameters. The system performance, including the dynamic response and steady-state error, will then be affected by these incorrect or inaccurate parameters. This problem mainly occurs in some complex systems or topologies where accurate system models or parameters are hard to get or predict. The system studied in this paper, an ac/dc three-phase two-level converter connected with a resistive load in Fig. 1, is a simple system whose parameters can be accurately measured. Also, because of the use of space voltage vectors, the switching frequency of MPC is not constant.

Section II outlines the system configuration and work principle of a three-phase ac/dc converter. The formulation and basic principle of the conventional MPPIC strategy is reviewed in Section III. The determination of the proposed MPSMC scheme, the design of the sliding surface, and the control law are discussed in Section IV. In Sections V and VI, the simulation and experimental results obtained from the MPSMC scheme are compared with those results from the MPPIC method under the same disturbance operational conditions, respectively. A short discussion of the simulation and experimental results is presented in Section VII. Finally, conclusions are drawn in Section VIII.

II. Modeling of an AC/DC Converter System

Fig. 1 illustrates the power circuit of a three-phase ac/dc converter, consisting of six insulated-gate bipolar transistor (IGBT) switches, $S_i (i = 1, 2, \ldots, 6)$. The main grid adopts the symmetrical three-phase three-wire system, connected with this IGBT full bridge through three series filter inductors with the same value L and resistors with the same value R. A capacitor C is connected on the dc side to filter the voltage harmonics.

The mathematical model of the ac/dc converter in the abc frame can be expressed as

$$\begin{bmatrix} L\frac{di_a}{dt} \\ L\frac{di_b}{dt} \\ L\frac{di_c}{dt} \\ C\frac{dV_{\rm dc}}{dt} \end{bmatrix} = \begin{bmatrix} -R & 0 & 0 & 0 \\ 0 & -R & 0 & 0 \\ 0 & 0 & -R & 0 \\ S_a & S_b & S_c & -1 \end{bmatrix} \begin{bmatrix} i_a \\ i_b \\ i_c \\ i_L \end{bmatrix} + \begin{bmatrix} V_{ga} - V_{ca} \\ V_{gb} - V_{cb} \\ V_{gc} - V_{cc} \\ 0 \end{bmatrix} \tag{1}$$

where V_{ga}, V_{gb}, and V_{gc} are the grid phase voltages; i_a, i_b, and i_c are the input currents of the converter; V_{ca}, V_{cb}, and V_{cc} are the converter input voltages; $V_{\rm dc}$ is the dc output voltage; i_L is the load current; S_a, S_b, and S_c stand for the switching state of the switches, respectively, and

$$S_k = \begin{cases} 1, & \text{upper switch on phase } k \text{ is ON} \\ 0, & \text{upper switch on phase } k \text{ is OFF} \end{cases} \tag{2}$$

where k stands for a, b, c phase. For example, $S_a = 1$ means S_1 ON and S_2 OFF.

The switching state can be expressed in the two-phase stationary $\alpha\beta$ orthogonal coordinate system as

$$\mathbf{S}_{\alpha\beta} = \begin{bmatrix} S_\alpha \\ S_\beta \end{bmatrix} = \frac{2}{3} \begin{bmatrix} 1 & -\frac{1}{2} & -\frac{1}{2} \\ 0 & \frac{\sqrt{3}}{2} & -\frac{\sqrt{3}}{2} \end{bmatrix} \begin{bmatrix} S_a \\ S_b \\ S_c \end{bmatrix}. \tag{3}$$

Based on the switching matrix, the dynamic model of the ac/dc converter input voltage can be represented with the dc-link voltage, as

$$\mathbf{V}_{\alpha\beta} = \begin{bmatrix} V_\alpha \\ V_\beta \end{bmatrix} = \mathbf{S} V_{\rm dc} = \begin{bmatrix} S_\alpha \\ S_\beta \end{bmatrix} V_{\rm dc}. \tag{4}$$

According to the principle of space vector PWM, the three-phase ac/dc converter input voltage can be controlled to eight voltage vectors onto a stationary two-axis reference frame (the $\alpha\beta$ coordinate system), as shown in Fig. 2 [26]. Note that V_0 and V_7 are zero voltage vectors.

The mathematical model dynamics are then represented in the $\alpha\beta$ orthogonal coordinates as

$$\mathbf{V}_{\mathbf{g},\alpha\beta} = L\frac{d\mathbf{i}_{\alpha\beta}}{dt} + R\mathbf{i}_{\mathbf{g},\alpha\beta} + \mathbf{V}_{\alpha\beta} \tag{5}$$

$$C\frac{dV_{\rm dc}}{dt} = \frac{3}{2}(i_{g,\alpha}S_\alpha + i_{g,\beta}S_\beta) - I_L \tag{6}$$

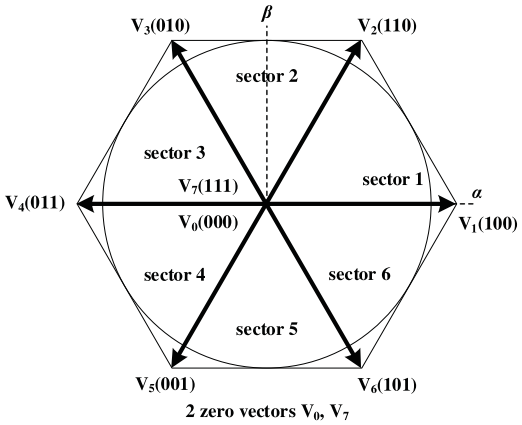

Fig. 2. Eight converter voltage vectors in the $\alpha\beta$ coordinate system.

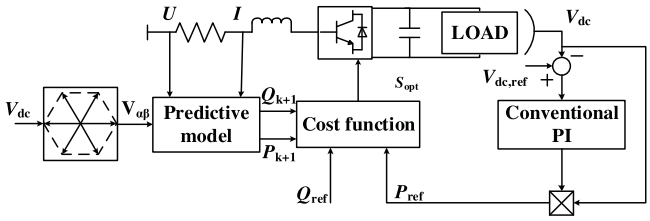

Fig. 3. Basic principle of the MPPIC method.

where $\mathbf{V}_{\mathbf{g},\alpha\beta}$ and $\mathbf{i}_{\mathbf{g},\alpha\beta}$ are the grid voltage and current vectors, respectively, and

$$\mathbf{V}_{\mathbf{g},\alpha\beta} = \begin{bmatrix} V_{g,\alpha} \\ V_{g,\beta} \end{bmatrix}, \quad \mathbf{i}_{\mathbf{g},\alpha\beta} = \begin{bmatrix} i_{g,\alpha} \\ i_{g,\beta} \end{bmatrix}.$$

Based on the analysis, the dynamic model of the ac/dc converter can be expressed with the $\alpha\beta$ axis components as

$$\begin{bmatrix} V_{g,\alpha} \\ V_{g,\beta} \end{bmatrix} = \begin{bmatrix} L & 0 \\ 0 & L \end{bmatrix} \begin{bmatrix} \frac{di_{g,\alpha}}{dt} \\ \frac{di_{g,\beta}}{dt} \end{bmatrix} + \begin{bmatrix} R & 0 \\ 0 & R \end{bmatrix} \begin{bmatrix} i_{g,\alpha} \\ i_{g,\beta} \end{bmatrix} + \begin{bmatrix} V_\alpha \\ V_\beta \end{bmatrix}. \quad (7)$$

III. Basic Principle of the MPPIC Scheme

The main purpose of MPC used in this paper is to control the active and reactive power flows to the desired values and in the desired direction, in addition to output voltage regulation. In the MPPIC scheme, a PI controller is applied to track the dc-link voltage to generate the active power reference, as shown in Fig. 3.

In the form of space vector equation, (7) can be rewritten as

$$\dot{\mathrm{x}} = A\mathrm{x} + B\mathrm{V}_{g,\alpha\beta} + D\mathrm{V}_{\alpha\beta} \quad (8)$$

where

$$\mathbf{x} = \mathbf{i}_{\mathbf{g},\alpha\beta} = \begin{bmatrix} i_{g,\alpha} \\ i_{g,\beta} \end{bmatrix}, \quad A = \begin{bmatrix} -\frac{R}{L} & 0 \\ 0 & -\frac{R}{L} \end{bmatrix},$$

$$B = \begin{bmatrix} \frac{1}{L} \\ 0 \end{bmatrix}, \quad D = \begin{bmatrix} -\frac{1}{L} \\ 0 \end{bmatrix}.$$

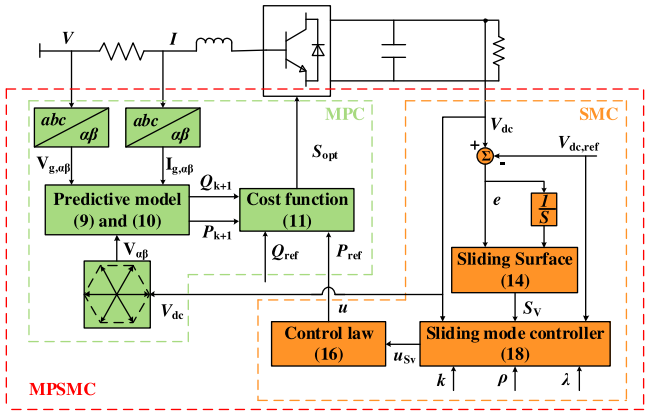

Fig. 4. Basic principle of the MPSMC scheme.

The discrete-time model of the grid current at the $(k+1)$th instant for a sample time T_s can be expressed as

$$\mathbf{i}_{\mathrm{g},\alpha\beta}(k+1) = \frac{T_s}{L}\left(\mathbf{V}_{\mathrm{g},\alpha\beta}(k) - R\mathbf{i}_{\mathrm{g},\alpha\beta}(k) - \mathbf{V}_{\alpha\beta}(k)\right) + \mathbf{i}_{\mathrm{g},\alpha\beta}(k). \quad (9)$$

Then, the active and reactive powers of this system can be calculated by

$$\begin{cases} P = \frac{3}{2}\mathrm{Re}\left\{V_g i_g^*\right\} = \frac{3}{2}(V_{g,\alpha} i_{g,\alpha} + V_{g,\beta} i_{g,\beta}) \\ Q = \frac{3}{2}\mathrm{Im}\left\{V_g i_g^*\right\} = \frac{3}{2}(V_{g,\beta} i_{g,\alpha} - V_{g,\alpha} i_{g,\beta}). \end{cases} \quad (10)$$

For the active and reactive power control, the cost function J can be defined as

$$J = \sqrt{(P - P_\mathrm{ref})^2 + (Q - Q_\mathrm{ref})^2} \quad (11)$$

where P_ref and Q_ref are the active and reactive power references, respectively.

It can be seen from (9) that the eight voltage vectors of the converter input voltage result in eight vectors of line current $\boldsymbol{i}_{g,\alpha\beta}$. Substituting (9) into (10), one can deduce eight possible values for the active and reactive powers. The cost function is employed to select the optimal voltage space vector that yields the P and Q with the minimum value of the cost function J, and this optimal switching vector (S_opt in Fig. 3) is then applied for the next step switching.

IV. Proposed MPSMC Scheme

The traditional PI controller has only one single set of unchangeable controller parameters during the operation. The system will suffer from slow dynamic performances when the system parameters and demands vary. On the contrary, the SMC has excellent dynamic performance, since the controller and the control law are both designed based on the system model. Taking advantage of this feature, the proposed MPSMC method applies a sliding-mode controller to replace the PI controller, as shown in Fig. 4. The control problem is to detect an appropriate control law so that the system state can track the expected active power and the desired dc-link voltage.

From Fig. 1, the instantaneous power ($P_{\rm i}$) conservation equation is used to describe the dynamic process of the dc-link voltage, which is

$$P_i = V_{\rm dc} i_{\rm dc} = CV_{\rm dc}\frac{d}{dt}V_{\rm dc} + \frac{1}{R_L}V_{\rm dc}^2. \tag{12}$$

By the principle of power equilibrium, the input instantaneous power of the converter is equal to its simultaneous output instantaneous power. The converter power loss is neglected in this paper. In the steady-state operation, the instantaneous power is equal to the active power, which is proportional to the voltage on the dc side. Therefore, in order to control the active power, the objective of SMC can be converted to control the dc-link voltage.

A. Active Power Sliding Surface

The control problem in the converter is to find a suitable control law so that the control variable $V_{\rm dc}$ can track the expected demand $V_{\rm dc,ref}$ accurately. To achieve this control target, the tracking error e_V can be defined as

$$e_V = V_{\rm dc} - V_{\rm dc,ref}. \tag{13}$$

To design the sliding surface, methods include a proportional of the error and a combination of the proportional and integral of the error. In this paper, to control the steady-state error to be zero, a linear combination of proportional and the integral of the designed voltage error is selected as the sliding surface [27]–[29], that is:

$$S_V = k_1 e_V + k_2 \int e_V\, dt = \lambda e_V + \int e_V\, dt = 0 \tag{14}$$

where $\lambda(\lambda = k_1/k_2)$ is a positive constant related to the time constant of the output voltage. Therefore, the response speed increases as λ is decreased, an idea originated from [30] but modified for the proposed controller. With such a relationship, a proper λ can be selected to optimize the dynamic and steady-state performances of the control system, such as the settling time, overshoot/undershoot, steady-state error, and control robustness.

Taking the derivative of S_V with respect to time and substituting (13) into (14), one obtains

$$\dot{S}_V = \lambda\left(\dot{V}_{\rm dc} - \dot{V}_{\rm dc,ref}\right) + V_{\rm dc} - V_{\rm dc,ref}. \tag{15}$$

B. Active Power Control Law

According to the inherent uncertainty with respect to the active power in this system, the control law can be designed as

$$u = \begin{cases} P_{\rm dc}^{+}(t), & S_V > 0 \\ P_{\rm dc}^{-}(t), & S_V < 0 \end{cases} \tag{16}$$

where u is the control law, and $P_{\rm dc}^{+}(t)$ and $P_{\rm dc}^{-}(t)$ represent the instantaneous power when the sliding variable reach different sides of the sliding-mode surface S_V, respectively. Fig. 4 depicts the control block diagram of the proposed MPSMC scheme.

According to (12) and (16), the first-order derivative of the dc-link voltage can be expressed as

$$\dot{V}_{\rm dc} = \frac{u}{CV_{\rm dc}} - \frac{1}{R_L C}V_{\rm dc} + \delta \tag{17}$$

where δ denotes the uncertainty disturbance on $V_{\rm dc}$.

Here, the bound of the uncertainty disturbance, ρ, is assumed to be $|\delta| \le \rho < 1$, i.e., ρ is a given positive constant.

Based on the aforementioned analysis, the controller can be designed as

$$u_{S_V} = CV_{\rm dc}\left[\left(\frac{1}{R_L C} - \frac{1}{\lambda}\right)V_{\rm dc} + \frac{1}{\lambda}V_{\rm dc,ref} - (\rho + k)\text{sign}(S_V)\right] \tag{18}$$

where $k > 0$ represents a suitable control gain.

C. Proof of Existence Condition

All the trajectory points in the vicinity of the sliding surface should reach the designed sliding surface within a finite time [31]. To guarantee this existence condition, one only needs to show that

$$\lim_{S_V \to 0} S \cdot \dot{S} < 0. \tag{19}$$

Substituting (17) and (18) into (15) yields

$$\dot{S}_V = -\lambda\left[(\rho + k)\text{sign}\,(S_V) - \delta\right]. \tag{20}$$

Multiplying $S_{\rm V}$ by (20), one obtains the sliding-mode existence condition as follows:

$$\begin{aligned} S_V\,\dot{S}_V &= S_V\left(-\lambda\left((\rho + k)\text{sign}\,(S_V) - \delta\right)\right) \\ &= -\lambda k\,|S_V| - \lambda S_V\,(\rho\,\text{sign}\,(S_V) - \delta). \end{aligned} \tag{21}$$

Therefore, the existence condition of the sliding mode can be satisfied with the following two cases [32].

Case 1: If the reaching point is in a positive position in the neighborhood field of the created switching surface, S_V, i.e., $S_V > 0$, then

$$\begin{aligned} S_V\,\dot{S}_V &= -\lambda k\,|S_V| - \lambda S_V\,(\rho\text{sign}\,(S_V) - \delta) \\ &= -\lambda k\,|S_V| - \lambda S_V\,(\rho - \delta) \\ &< -\lambda k\,|S_V| \\ &< 0. \end{aligned} \tag{22}$$

This leads to

$$\lim_{S_V \to 0^+} S_V\,\dot{S}_V < 0. \tag{23}$$

Case 2: If the reaching point is in a negative position in the neighborhood field of the created switching surface, S_V, i.e., $S_V < 0$, then

$$\begin{aligned} S_V\,\dot{S}_V &= -\lambda k\,|S_V| - \lambda S_V\,(\rho\text{sign}\,(S_V) - \delta) \\ &= -\lambda k\,|S_V| + \lambda S_V\,(\rho + \delta) \\ &< -\lambda k\,|S_V| \\ &< 0. \end{aligned} \tag{24}$$

This results in

$$\lim_{S_V \to 0^-} S_V \dot{S}_V < 0. \tag{25}$$

From (23) and (25), one can conclude that (19), the existence condition, can be satisfied by selecting the proper sliding coefficients, λ and k.

D. Proof of the Tracking Condition

The tracking condition of the sliding mode can be derived by applying the Lyapunov stability analysis [25], [26]. For this analysis, a Lyapunov function candidate is designed as

$$V_{S_V}(V_{\rm dc}) = \frac{S_V^2}{2}. \tag{26}$$

It is positive for any reaching points, expected for the equilibrium point $V_{\rm dc} = V_{\rm dc,ref}$. Only when the sliding variable reaches the equilibrium point, the Lyapunov function V_{Sv} will be zero. Hence, the proposed Lyapunov function V_{Sv} is positive definite.

Based on (23) and (25), the derivative of V_{Sv} with respect to time can be obtained as

$$\dot{V}_{S_V}(V_{\rm dc}) = S_V \dot{S}_V < 0. \tag{27}$$

Therefore, the derivative of V_{Sv} is negative definite.

Theorem: If a Lyapunov function V is positive definite and its derivative is negative definite, the system is asymptotically stable at the equilibrium point.

As a result, the designed Lyapunov function V_{Sv} complies with the robustness of Lyapunov stability analysis. Moreover, the system stables at the equilibrium point ($V_{\rm dc,ref}$), which can be expressed as

$$P_{\rm ac} = P_{\rm dc} = V_{\rm dc} I_{\rm dc} = \frac{V_{\rm dc,ref}^2}{R_L}. \tag{28}$$

Substituting (18) into (17) reveals that when the system trajectory points reach the sliding surface, i.e., $S_V = 0$, the uncertainty disturbance is equal to zero as well, i.e., $\delta = 0$. Then, the first-order derivative of the voltage error with respect to time can be rewritten as

$$\dot{e}_V = \dot{V}_{\rm dc} - \dot{V}_{\rm dc,ref} = -\frac{1}{\lambda}(V_{\rm dc} - V_{\rm dc,ref}). \tag{29}$$

According to (29), as long as the sliding coefficient λ is positive, the trajectory points can keep stable at the sliding surface theoretically. However, as the ac/dc converter is a nonlinear system, a positive λ can hardly guarantee that all the reaching points satisfy the stability condition, except for those points from the vicinity of the stability field. By applying the MPC and SMC schemes simultaneously in this system, all the trajectory points can hit and remain stable at the designed sliding surface only when λ is chosen from an inherent range of the analyzed set, i.e., $\lambda > 0$.

Based on the aforementioned analysis, the nonlinear criteria to choose the switching state should be as follows.

1) If $V_{\rm dc} > V_{\rm dc,ref} \Rightarrow \dot{V}_{\rm dc} < 0 \Rightarrow$ therefore choose a switching state suitable to decrease $V_{\rm dc}$.
2) If $V_{\rm dc} < V_{\rm dc,ref} \Rightarrow \dot{V}_{\rm dc} > 0 \Rightarrow$ therefore choose a switching state suitable to increase $V_{\rm dc}$.
3) If $V_{\rm dc} = V_{\rm dc,ref} \Rightarrow \dot{V}_{\rm dc} = 0 \Rightarrow$ therefore choose a switching state that does not significantly change $V_{\rm dc}$.

TABLE I
ELECTRIC PARAMETERS OF THE AC/DC CONVERTER

Symbol	Quantity	Value
L	Filter inductance	20 mH
C	Filter capacitor	680 μF
$R_{\rm L}$	Load resistance	140 Ω
$V_{\rm LL}$	Grid line-line voltage (RMS)	50 V
f	Gird frequency	50 Hz
$V_{\rm dc}$	DC output voltage	150 V
$T_{\rm S}$	Sample time	50 μs

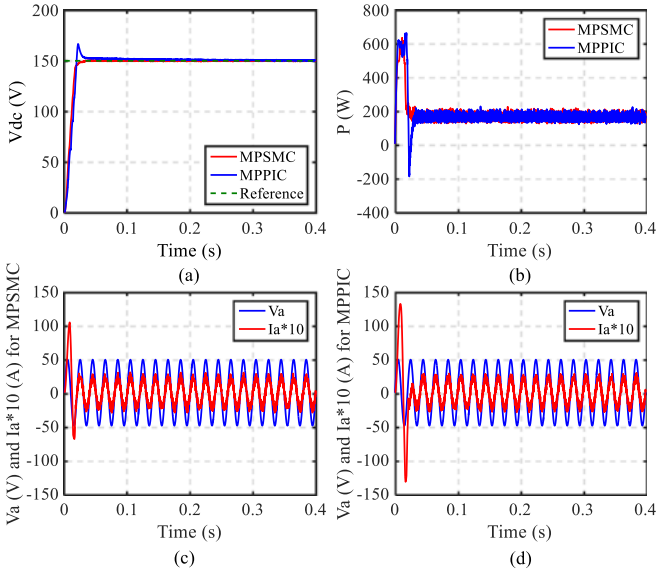

Fig. 5. Steady-state and dynamic performances. (a) DC voltage. (b) Active power. (c) Instantaneous voltage and current of phase A under MPSMC. (d) Instantaneous voltage and current of phase A under MPPIC.

V. SIMULATION RESULTS

A. Converter Parameters

This section provides the simulation results obtained from the standard MPPIC and the proposed MPSMC schemes. The simulations have been carried out in a MATLAB/Simulink environment with a detailed ac/dc converter configuration of Fig. 1. Table I shows the simulation operation and electric parameters of the converter. It should be noted that when the desired dc-link voltage is 150 V and the resistive load is 140 Ω, the active power equals 161 W. The reference reactive power, $Q_{\rm ref}$, is set to be 0 var during all the simulation testing to ensure a unity power factor operation. Note that taking the overshoot and response time into consideration, a proper pair of PI parameters is chosen in the following simulation and experimental tests.

B. Start-Up Dynamic and Steady-State Performance

Fig. 5 shows the start-up and steady-state responses of the converter controlled by the MPSMC and MPPIC methods,

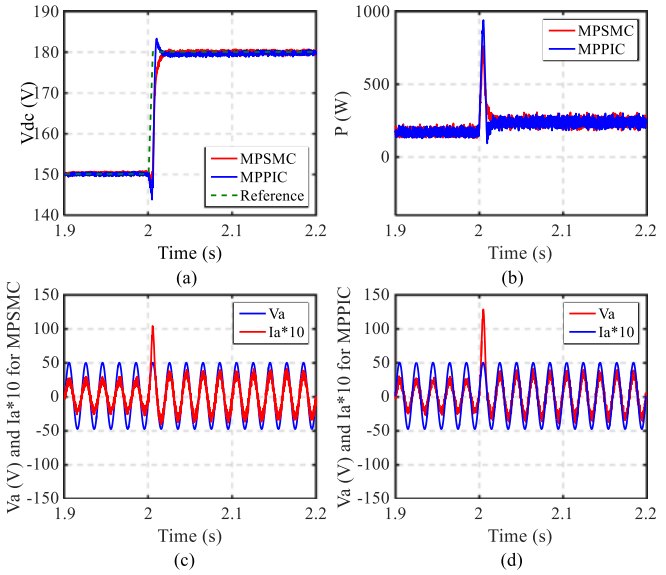

Fig. 6. Responses to an unexpected increase of dc voltage demand. (a) DC voltage. (b) Active power. (c) Phase A voltage and current under MPSMC. (d) Phase A voltage and current under MPPIC.

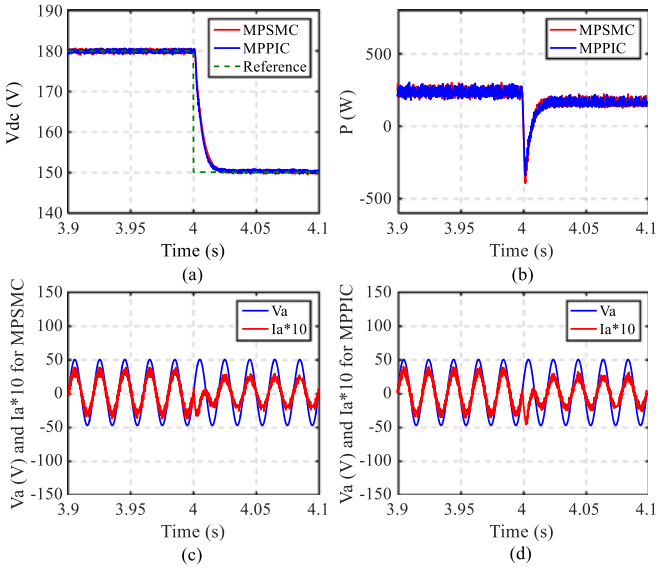

Fig. 7. Responses to an unexpected drop of dc voltage demand. (a) DC voltage. (b) Active power. (c) Phase A voltage and current under MPSMC. (d) Phase A voltage and current under MPPIC.

separately, to regulate the dc-link voltage at 150 V. As shown in Fig. 5(a), both methods can control the voltage to the reference value as required, but the converter controlled by MPSMC can track the reference voltage much faster than that controlled by MPPIC. The settling time, which is defined as the time required to reach zero steady-state error, is about 0.03 s under MPSMC, which is only 8.57% of 0.35 s, the settling time under MPPIC. Compared with the 9.13% output voltage overshoot obtained by the conventional MPPIC scheme, the output voltage overshoot can be almost eliminated by using MPSMC.

As also shown in Fig. 5(b), the active power under MPSMC responds much faster than that under MPPIC and has almost no undershoot, while both MPSMC and MPPIC deliver similar steady performance. Fig. 5(c) and (d) illustrates the performances of phase A grid current under MPSMC and MPPIC, respectively. The ac current under MPSMC takes around one cycle time to reach the steady state, whereas the conventional MPPIC algorithm uses about 1.50 cycle time to reach the steady state with an overshoot much bigger than that under MPSMC. The ac current responding speed has been increased by approximately one-third, or 33.33%.

C. Operation Under Load Voltage Demand Variation

Fig. 6 shows the dynamic performances to an unexpected increase of dc voltage demand under MPSMC and MPPIC, separately. The dc-link voltage is stepped up from 150 to 180 V at $t = 2$ s. As shown in Fig. 6(a), under the standard MPPIC, it takes 0.10 s to reach the new operation state with no steady-state error, which is almost three times longer than that under the proposed MPSMC. On the other hand, the dc-link voltage tracks the reference value with almost no overshoot under MPSMC, while under MPPIC, there is an apparent overshoot of 1.78%.

Fig. 6(b) shows the much faster the active power dynamic response before reaching the steady-state value of 131 W under MPSMC than that under MPPIC. Fig. 6(c) and (d) presents similar dynamic and steady-state performances of ac currents obtained under MPSMC and MPPIC, respectively.

Compared to the response when a step change is applied in the dc voltage, similar dynamic and steady-state performances can also be achieved when a suddenly drop voltage is imposed. In Fig. 7(a) and (b), both the dc voltage and active power obtained from the proposed MPSMC and the standard MPPIC schemes can track the reference values and reach the updated steady states. Fig. 7(c) and (d) shows the similar dynamic performances of grid currents obtained from two strategies, respectively.

D. Operation Under Load Resistance Variation

A sharp load resistance decrement from 280 to 140 Ω at time instant 2 s is applied to the system, as illustrated in Fig. 8. By following the designed control law based on the system model, the output voltage can avoid excessive distortion in MPSMC. Although the MPPIC can recover to the original voltage within a finite time length, the settling time, equal to 0.6 s, is much longer than the proposed method, and the undershoot, equal to 2%, can hardly be avoided. The proposed MPSMC performance exhibits a fast response with no undershoot on the load voltage, as well as the active power, as illustrated in Fig. 8(a) and (b). Note that the transient currents on the grid side obtained from the MPSMC and MPPIC strategies present similar performance in Fig. 8(c) and (d), respectively.

VI. Experimental Results

A laboratory prototype of the ac/dc converter, as shown in Fig. 9, is developed to verify the proposed MPSMC and the MPPIC schemes. A three-phase variac is used to achieve a 50-V/50-Hz power supply voltage. A 6MBP50RA-060-55 three-phase IGBT module from Fuji Electric is used as the

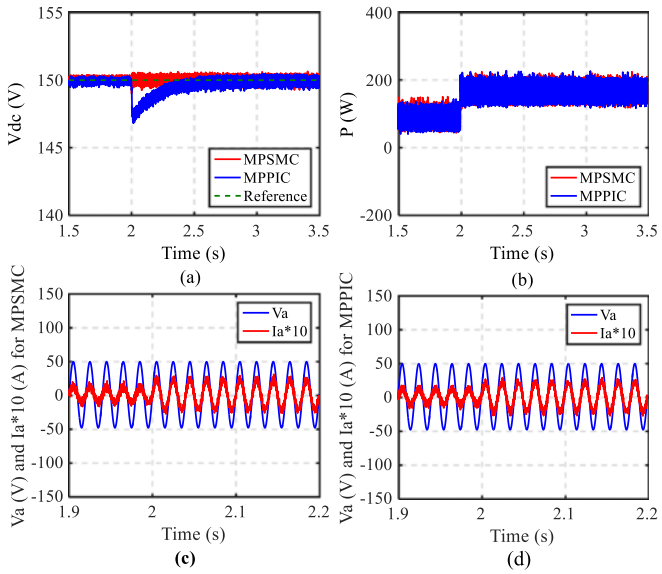

Fig. 8. Unexpected load variation condition. (a) DC voltage. (b) Active power. (c) Instantaneous voltage and current of phase A in MPSMC. (d) Instantaneous voltage and current of phase A in MPPIC.

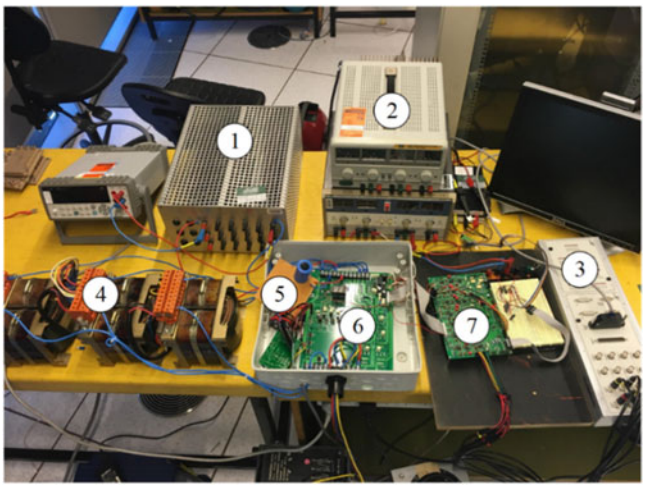

Fig. 9. Experimental setup of the ac/dc converter: (1) dc resistive load, (2) dc power supply, (3) dSPACE, (4) inductors, (5) dc capacitor C, (6) ac/dc converter, and (7) control unit.

three-phase ac/dc converter. A 680-μF dc capacitor and a 140-Ω resistive load with a current limitation of about 1.5 A are connected in parallel on the dc side. The experimental tests are performed under the same conditions as the simulation, and with the same parameters as listed in Table I. Four LEM voltage sensors (LEM LV 25-P) and three LEM current sensors (LEM LA 25-NP) are used to measure the dc-link voltage, grid voltages, and grid currents, respectively.

The experimental tests of the proposed MPSMC and the conventional MPPIC methods are carried out by applying the real-time interface system dSPACE with a DS1104 control desk. This control desk works together with MATLAB/Simulink-R2009. Both control schemes are implemented in C language, and the computations are performed on the dSPACE DS1104 controller board. The sampling frequency is 10 kHz in the experimental tests. The data recording and reference values are observed and set via the dSPCE ControlDesk environment. The experimental results are obtained for both MPSMC and MPPIC schemes during various disturbance operations. The reactive power is set to 0 var to achieve a unit power factor. Since it takes a long time for the system to reach the new operation with no steady-state error by using the conventional MPPIC method, the response time for the MPPIC scheme in the following experimental results is realistically defined as the time for the system to reach a new operating condition within 1% steady-state error.

A. Selection of PI Parameters for the MPPIC Method

In order to choose the best MPPIC method performances to compare with MPSMC, the standard rule to design the PI controller proportional and integral parameters, denoted as K_p and K_i, respectively, is used in this paper [33].

A parameter z defined as

$$z = \frac{V_{\rm dc}^2}{2} \tag{30}$$

is introduced to analyze the system plant.

Then, the first-order derivation of z can be written as

$$\dot{z} = V_{\rm dc}\dot{V}_{\rm dc}. \tag{31}$$

Equation (12) can then be rewritten as

$$P_{\rm ref} = C\dot{z} + \frac{2z}{R_L}. \tag{32}$$

The system plant can be expressed as

$$G(s) = \frac{z}{P_{\rm ref}} = \frac{\frac{R_L}{2}}{\frac{R_L C}{2}s + 1}. \tag{33}$$

Based on the standard rules in [33, Table 4.5], the rate of $K_{\rm p}/K_{\rm i}$ is calculated by using

$$\frac{K_p}{K_i} = \frac{\xi^2 R_L^2 C}{\left(1 + \frac{R_L}{2}\right)^2} \tag{34}$$

where ξ is the damping ratio of the system and recommended to be set as 0.707.

Based on this design principle, the PI parameters K_p and K_i are fine tuned for each specific operation condition. The selection process is analyzed and the obtained dc-link voltage performances with different controller parameter values are compared.

Fig. 10 shows the different voltage performances with varying K_p values and a constant K_i. With the same reference, the overshoot and response time will be affected by the gains of the PI controller. As shown in Fig. 10, the output voltage can reach the reference value much faster with a larger proportional part. On the other hand, this increased K_p leads to an overshoot on the voltage. Taking both the overshoot and response times into consideration, an appropriate K_p, which equals 0.15, is selected for this test.

Once the gain of K_p is adopted, the integral parameter K_i is chosen based on the steady-state error and the oscillation. It can be observed from Fig. 11 that the dc voltage is able to achieve the target under different K_i gains. The steady-state error is kept

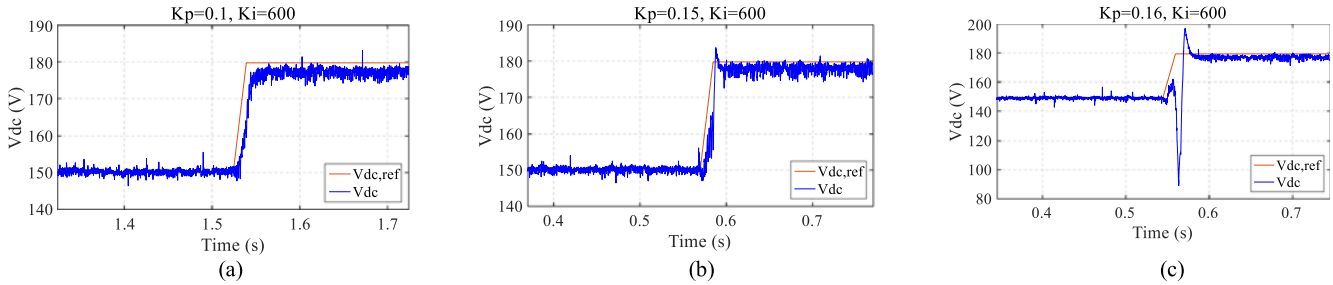

Fig. 10. $V_{\rm dc}$ performances with different K_p gains for voltage variation operations.

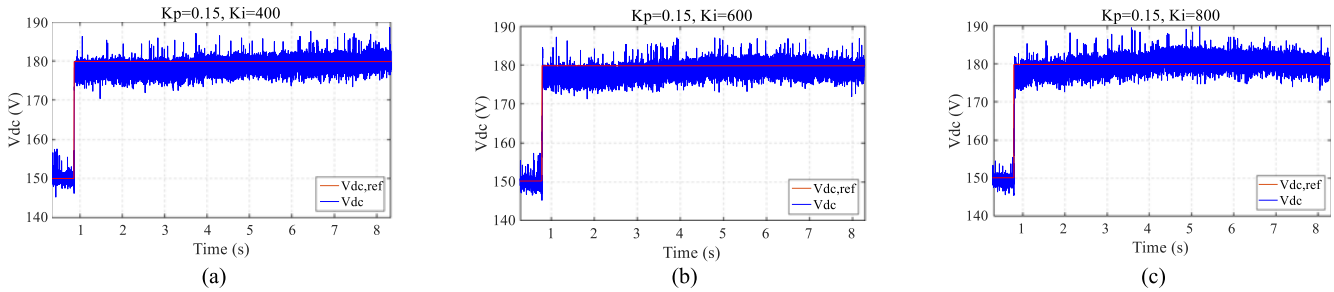

Fig. 11. $V_{\rm dc}$ response to voltage demand step increase with different K_i gains.

within 2% of the expected value. However, when the K_i is small, as shown in Fig. 11(a), the output keeps increasing to reach the reference without any error. This takes a long settling time for the system. While with a larger value of K_i in Fig. 11(c), this yields a faster response, but also a larger amplitude of oscillation. Considering these two factors, a K_i coefficient of 600 is devised for this system. Therefore, a PI controller with K_p and K_i, equal to 0.15 and 600, respectively, is designed for voltage variation operations.

It is noticeable that if the same parameters are used in load variation operation, as described in Fig. 12(a), the undershoot is comparatively large, which is not the best performance for MPPIC. From Fig. 12, it can be seen that the larger coefficient K_p the system has, the less undershoot the dc-link voltage will perform, as long as the system is stable. Therefore, the K_p with 0.3 is tuned manually to get better performances in the load variation comparison study. Based on the above analysis, it can be seen that automatic tuning is significant and necessary for the PI controller to achieve better steady and dynamic performances.

The oscillations that are observed in Figs. 10–12 are due to the background noise, analog-to-digital conversion error, limited vectors in the MPC method, and certain uncontrollable practical factors.

B. Comparison of MPSMC and MPPIC Schemes

The dynamic performances of the standard and proposed methods with the dc-link voltage demand variations are experimentally compared in Figs. 13 and 14. It can be seen clearly that the output dc-link voltage can be regulated to the desired value by both proposed MPSMC and traditional MPPIC methods. The dc voltage reference steps from 150 to 180 V at 0.3374 s. It takes 0.0177 s for the system controlled by the proposed MPSMC method to reach the new steady state, which is much shorter than 0.0253 s by the conventional MPPIC scheme with 1% steady-state error. The response time has been reduced by 30%. From Fig. 13(b), it can be observed that there is an obvious overshoot of the dc-link voltage by using the traditional method. Similar performances of active and reactive powers for both schemes are illustrated in Fig. 13(c) and (d), respectively. For both two algorithms, an overshoot is introduced on the active power and the PQ coupling cannot be eliminated. When the active power increases, there is an obvious spike on the reactive power obtained from the MPPIC strategy. Fig. 13(e) and (f) depicts the grid currents of phase A for the two control strategies. The current dynamic response obtained by the MPSMC method also presents a much faster speed than that by the MPPIC method. The grid current response time is similar to that for the dc voltage obtained from the corresponding scheme within 1% steady-state error.

Fig. 14 presents the dynamic and steady performances of the two methods when a reduction of the voltage demand is applied. The dc voltage obtained from MPPIC has a steady-state error of approximately 1.3% for the operating point, while the error for MPSMC is zero. This means that a much longer response time is required for MPPIC to track the reference value with zero steady-state error. The reason of this steady-state error is that the PI control parameters are selected to ensure that the system will operate effectively when a 180-V voltage reference is employed. During the operation, this pair of parameters is fixed and constant. However, these selected parameters are not the best choice for the new working condition when the voltage reference is reduced to 150 V. It is impossible for them to be tuned automatically based on different operations, which leads to a

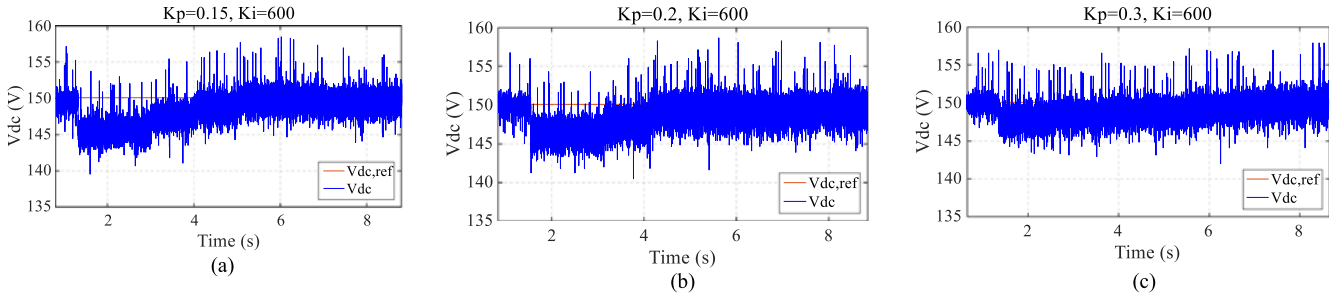

Fig. 12. V_{dc} performances with different K_p gains for the load variation operation.

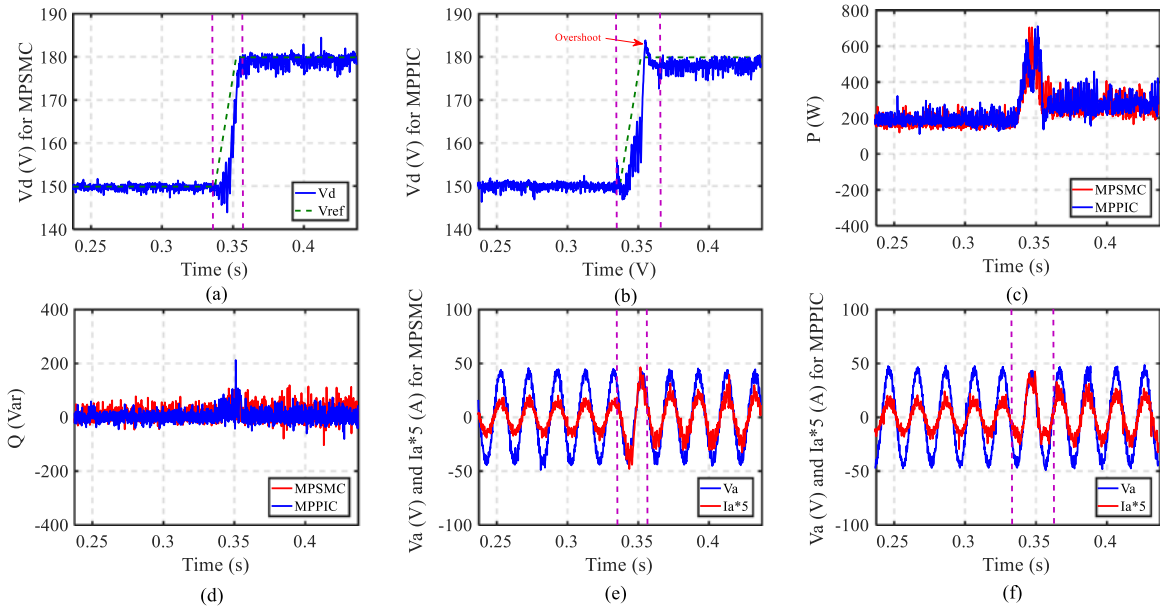

Fig. 13. Experimental results of sudden increase of dc voltage. (a) DC voltage of MPSMC. (b) DC voltage of MPPIC. (c) Active power. (d) Reactive power. (e) Instantaneous voltage and current of phase A in MPSMC. (f) Instantaneous voltage and current of phase A in MPPIC.

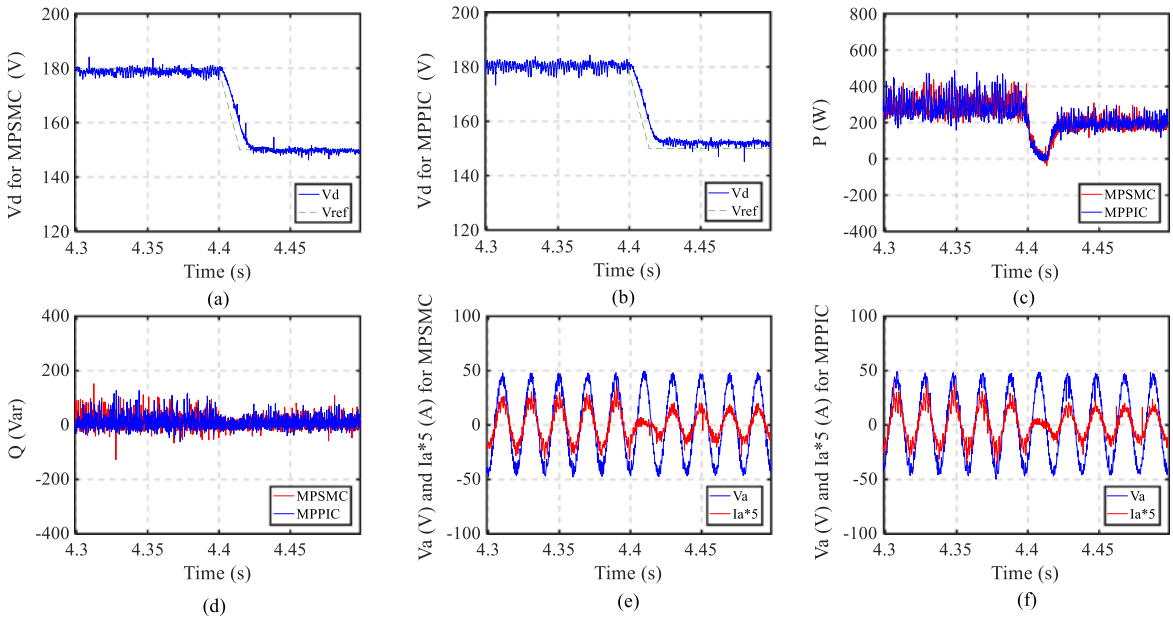

Fig. 14. Experimental results of unexpected decrease demand of dc voltage. (a) DC voltage of MPSMC. (b) DC voltage of MPPIC. (c) Active power. (d) Reactive power. (e) Instantaneous voltage and current of phase A in MPSMC. (f) Instantaneous voltage and current of phase A in MPPIC.

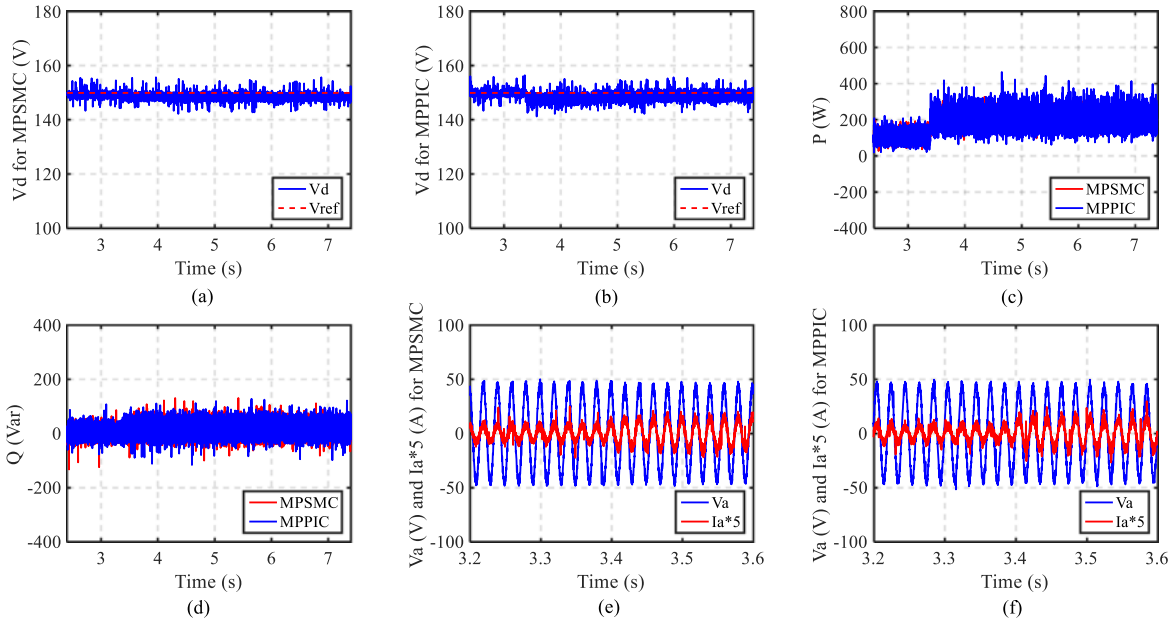

Fig. 15. Experimental results of unexpected increase demand of dc voltage. (a) DC voltage of MPSMC. (b) DC voltage of MPPIC. (c) Active power. (d) Reactive power. (e) Instantaneous voltage and current of phase A in MPSMC. (f) Instantaneous voltage and current of phase A in MPPIC.

long response time. Compared with the dynamic performances of MPPIC, similar performances of active power, reactive power, and ac current are shown in Fig. 14(c)–(f), respectively. With the selected PI parameters, the system voltage inclines to decrease rather than increase, which yields no overshoot. Therefore, the current during the voltage drop operation is different from that during the voltage increase operation, which can also be proved in the simulation result.

The dynamic responses to the external load disturbance by applying MPSMC and MPPIC strategies are exhibited in Fig. 15, where the external load is suddenly changing from 280 to 140 Ω at time instant 3.399 s. As the sliding surface is designed based on the model, the dc-link voltage can reach the new steady state almost immediately, as shown in Fig. 15(a). Fig. 15(b) shows the experimental dc-link voltage waveform for the conventional MPPIC. It has an undershoot of the dc voltage and takes around 1.5 s to track the reference after the load variation. It can be verified that the control performance by using the proposed method is improved, since the undershoot can be eliminated. Fig. 15(c)–(f) shows that the dynamic performances for active power and grid current are much similar for both schemes, respectively.

VII. Discussion

Table II summarizes the settling time of simulation and experimental tests by using the proposed MPSMC and MPPIC algorithms. The response time for the simulation results is from the starting point to the steady point when the output hits the reference with no steady-state error. For the experimental results, due to the signal transmission and acquisition, the settling time with no steady-state error is longer than the simulation results. In order to analyze the dynamic performance, the response time is defined from the starting point to the final point within 1% steady-state error for voltage variation operations. Therefore, the results obtained from the experimental tests are much shorter than those from the simulation test during voltage varying operation. It can be seen from Table II that the settling times obtained from MPSMC are much shorter than that from MPPIC for both simulation and experimental tests. For the load variation operation, in order to observe the steady-state performance, the settling time is compared when the output hits the reference value with no error. As shown by both simulation and experimental results, the proposed MPSMC exhibits better performance than the traditional MPPIC. Due to the use of space voltage vectors, the switching frequencies for both MPPIC and MPSMC methods are not constant.

TABLE II
Settling Time for Simulation and Experimental Tests

Operation	Control schemes	MPSMC	MPPIC
Voltage increase	Simulation results	0.03 s	0.35 s
	Experimental results (Within 1% steady-state error)	0.0177 s	0.0253 s
Voltage decrease	Simulation results	0.025 s	0.025 s
	Experimental results (Within 1% steady-state error)	0.02 s	0.03 s
Load variation	Simulation results	$<$0.01 s	0.6 s
	Experimental results (Steady-state error is 0)	$<$0.1 s	1.5 s

There is an inrush current in the simulation results of MPSMC or MPPIC, as shown in Fig. 5. The reason is that the grid source with a 50-V amplitude was connected all the time. When we started the system, there was an inrush current at the beginning. In the experiment, for safety reason, a variac is connected between the power grid and the system. The voltage increases slowly from 0 V to the expected value. By increasing the power

supply slowly, the inrush current can be limited. However, since the actual system will be connected to the power grid directly, it will cause a large inrush current that may destroy or reduce the lifetime of the semiconductor as well as false-trigger the protection circuit in the ac power supply. Nevertheless, a bypass diode or a soft-start procedure can be added in this situation to reduce and limit the inrush current.

VIII. Conclusion

In this paper, a novel MPSMC technique is proposed and implemented for an ac/dc converter. The proposed control method is compared with an MPPIC, which is based on the system model and the designed cost function. According to the objectives and parameter references, it is possible to select an optimal switching state to achieve the target. The PI controller is applied to generate the active power reference in the control loop. During the operation, the system will encounter some transient disturbances, such as voltage and load demand variations. However, the parameter values of the PI controller are constant, which is hard to adjust along with system disturbances. MPSMC combines the main advantages of an MPPIC and SMC schemes, such as the ability to achieve multiobjective control and simple implement. The designed surface of SMC is based on the system model. This design can help it track the references and load resistance much more accurately and faster. The proposed MPSMC method is validated by extensive simulation and experimental testing in comparison with MPPIC. The results show that with the same demand variation, the MPSMC technique has a faster dynamic response and no steady-state error of the dc-link voltage compared with the MPPIC scheme. The effect of improvements depends on the variations of different system disturbances and demands. On the other hand, the dynamic and steady-state performances of active power, reactive power, and grid currents obtained from MPSMC are much better than those achieved from MPPIC.

References

[1] M. Kesler, M. C. Kisacikoglu, and L. M. Tolbert, "Vehicle-to-grid reactive power operation using plug-in electric vehicle bidirectional offboard charger," *IEEE Trans. Ind. Electron.*, vol. 61, no. 12, pp. 6778–6784, Dec. 2014.

[2] P. Cortes, J. Rodrigues, and D. E. Quevedo, "Predictive current control strategy with imposed load current spectrum," *IEEE Trans. Power Electron.*, vol. 23, no. 2, pp. 612–618, Nov. 2008.

[3] Q. Xu *et al.*, "Analysis and comparison of modular railway power conditioner for high-speed railway traction system," *IEEE Trans. Power Electron.*, vol. 32, no. 8, pp. 6031–6048, Aug. 2017.

[4] H. Zhao and L. Cheng, "Open switch fault diagnostic method for back to back converters of doubly fed wind power generation system," *IEEE Trans. Power Electron.*, 2017, to be published, doi: 10.1109/TPEL.2017.2705985.

[5] M. Davari, "Robust multi-objective control of VSC-based dc-voltage power port in hybrid ac/dc multi-terminal micro-grids," *IEEE Trans. Smart Grid*, vol. 4, no. 3, pp. 1597–1612, Mar. 2013.

[6] Y. Li, X. Shi, and B. Liu, "Development, demonstration, and control of a testbed for multiterminal HVDC system," *IEEE Trans. Power Electron.*, vol. 32, no. 8, pp. 6069–6078, Aug. 2017.

[7] S. K. Kim, D. K. Choi, and K. B. Lee, "Offset-free model predictive control for the power control of three-phase AC/DC converters," *IEEE Trans. Power Electron.*, vol. 62, no. 11, pp. 7114–7126, Nov. 2015.

[8] D. E. Quevedo, P. Aguilera, and M. A. Perez, "Model predictive control of an AFE rectifier with dynamic references," *IEEE Trans. Power Electron.*, vol. 27, no. 7, pp. 612–618, Nov. 2012.

[9] S. C. Shin, H. J. Lee, and Y. H. Kim, "Transient response improvement at startup of a three-phase AC/DC converter for a DC distribution system in commercial facilities," *IEEE Trans. Power Electron.*, vol. 29, no. 12, pp. 6742–6753, Dec. 2014.

[10] J. Liu, Y. Gao, and W. Luo, "Takagi–Sugeno fuzzy-model-based control of three-phase AC/DC voltage source converters using adaptive sliding mode technique," *IET Control Theory Appl.*, vol. 11, no. 8, pp. 1255–1263, Dec. 2016.

[11] R. Kadri, J. P. Gaubert, and G. Champenois, "An improved maximum power point tracking for photovoltaic grid-connected inverter based on voltage-oriented control," *IEEE Trans. Ind. Electron.*, vol. 58, no. 1, pp. 66–75, Jan. 2011.

[12] W. Shireen, R. A. Kulkari, and M. Arefeen, "Analysis and minimization of input ripple current in PWM inverters for designing reliable fuel cell power systems," *J. Power Sources*, vol. 156, no. 2, pp. 448–454, Jun. 2006.

[13] J. Dannehl, C. Wessels, and F. W. Fuchs, "Limitations of voltage-oriented PI current control of grid-connected PWM rectifiers with LCL filters," *IEEE Trans. Ind. Electron.*, vol. 56, no. 2, pp. 380–388, Feb. 2009.

[14] Y. Zhang, W. Xie, and Z. Li, "Model predictive direct power control of a PWM rectifier with duty cycle optimization," *IEEE Trans. Power Electron.*, vol. 28, no. 11, pp. 5343–5351, Nov. 2013.

[15] Y. Cho and K. B. Lee, "Virtual-flux-based predictive direct power control of three-phase PWM rectifiers with fast dynamic response," *IEEE Trans. Power Electron.*, vol. 31, no. 4, pp. 3348–3359, Apr. 2016.

[16] J. Han, S. K. Solanki, and J. Solanki, "Coordinated predictive control of a wind/battery microgrid system," *IEEE J. Emerg. Sel. Topics Power Electron.*, vol. 1, no. 4, pp. 296–305, Dec. 2013.

[17] Y. Zhang and C. Qu, "Direct power control of a pulse width modulation rectifier using space vector modulation under unbalanced grid voltages," *IEEE Trans. Power Electron.*, vol. 30, no. 10, pp. 5892–5901, Oct. 2015.

[18] D. K. Choi and K. B. Lee, "Dynamic performance improvement of AC/DC converter using model predictive direct power control with finite control set," *IEEE Trans. Ind. Electron.*, vol. 62, no. 2, pp. 757–767, Feb. 2015.

[19] S. Kwak and J. C. Park, "Model-predictive direct power control with vector preselection technique for highly efficient active rectifiers," *IEEE Trans. Ind. Informat.*, vol. 11, no. 1, pp. 44–52, Sep. 2015.

[20] J. Ma, W. Song, and S. Jiao, "Power calculation for direct power control of single-phase three-level rectifiers without phase-locked loop," *IEEE Trans. Ind. Electron.*, vol. 63, no. 5, pp. 2871–2882, May 2016.

[21] J. Knight, S. Shirsavar, and W. Holderbaum, "An improved reliability Cuk based solar inverter with sliding mode control," *IEEE Trans. Power Electron.*, vol. 21, no. 4, pp. 1107–1115, Jul. 2006.

[22] D. Cao and J. Fei, "Adaptive fractional fuzzy sliding mode control for three-phase active power filter," *IEEE Access*, vol. 4, pp. 6645–6651, 2016.

[23] F. Sebaaly, H. Vahedi, and H. Y. Kanaan, "Sliding mode fixed frequency current controller design for grid-connected NPC inverter," *IEEE J. Emerg. Sel. Topics Power Electron.*, vol. 4, no. 4, pp. 1397–1405, Oct. 2016.

[24] J. J. More, P. F. Puleston, and C. Kunusch, "Development and implementation of a supervisor strategy and sliding mode control setup for fuel-cell-based hybrid generation systems," *IEEE Trans. Energy Convers.*, vol. 30, no. 1, pp. 218–225, Mar. 2015.

[25] X. Zhang, L. Sun, and K. Zhao, "Nonlinear speed control for PMSM system using sliding-mode control and disturbance compensation techniques," *IEEE Trans. Power Electron.*, vol. 28, no. 3, pp. 1358–1365, Mar. 2013.

[26] M. P. Akter, S. Mekhilef, and N. M. L. Tan, "Modified model predictive control of a bidirectional AC–DC converter based on Lyapunov function for energy storage systems," *IEEE Trans. Ind. Electron.*, vol. 63, no. 2, pp. 704–715, Feb. 2016.

[27] N. Derbel, J. Ghommam, and Q. Zhu, *Applications of Sliding Mode Control (Studies in Systems, Decision and Control)*, vol. 79, N. Derbel, Ed., 1st ed. Singapore: Springer, 2017, pp. 335–337. [Online]: http://http://libgen.io/search.php?req=Applications+of+Sliding+Mode+Control&lg_topic=libgen&open=0&view=simple&res=25&phrase=1&column=def

[28] O. L. Santos, L. M. Salamero, and G. Garcia, "Robust sliding-mode control design for a voltage regulated quadratic boost converter," *IEEE Trans. Power Electron.*, vol. 30, no. 4, pp. 2313–2327, Apr. 2015.

[29] J. Lee, S. Khoo, and Z. Wang, "DSP-based sliding-mode control for electromagnetic-levitation precise-position system," *IEEE Trans. Ind. Informat.*, vol. 9, no. 2, pp. 817–827, May 2013.

[30] J. F. Silva, "Sliding-mode control of boost-type unity-power-factor PWM rectifiers," *IEEE Trans. Ind. Electron.*, vol. 46, no. 3, pp. 594–603, Jun. 1999.
[31] S. Li, M. Li, and X. Yu, "Design and implementation of terminal sliding mode control method for PMSM speed regulation system," *IEEE Trans. Ind. Informat.*, vol. 9, no. 4, pp. 1879–1891, Nov. 2013.
[32] T. He, L. Li, and J. Zhu, "A novel model predictive sliding mode control for AC/DC converters with output voltage and load resistance variations," in *Proc. IEEE Energy Convers. Congr. Expo.*, Milwaukee, WI, USA, Sep. 18–22, 2016, pp. 1–6.
[33] M. P. Kazmierkowski, F. Blaabjerg, and R. Krishnan, *Control Power Electronics: Selected Problems*. San Francisco, CA, USA: Academic, 2002, pp. 117–121.

Tingting He (S'14) received the B.S. and master's degrees in electrical engineering from Beijing Jiaotong University, Beijing, China, in 2009 and 2015, respectively. She is currently working toward the Ph.D. degree at the School of Electrical and Data Engineering, The University of Technology Sydney, Sydney, NSW, Australia.

Her research interests include power electronics, electric vehicles, and predictive control.

Dylan Dah-Chuan Lu (M'04–SM'09) received the B.E. and Ph.D. degrees from The Hong Kong Polytechnic University, Hong Kong, in 1999 and 2004, respectively, both in Electronic and Information Engineering.

In 2003, he joined PowereLab Ltd. as a Senior Design Engineer and was responsible for industrial switching power supply projects. He was a full-time faculty member with The University of Sydney from 2006 to 2016. He now holds an honorary position with the University of Sydney. Since July 2016, he has been an Associate Professor at the School of Electrical and Data Engineering, University of Technology Sydney, Sydney, NSW, Australia. His current research interests include efficient and reliable power conversion for renewable sources, energy storage systems, and microgrids.

Dr. Lu is a member of Engineers Australia. He was a recipient of the Best Paper Award in the category of Emerging Power Electronic Technique at the 2015 IEEE International Conference on Power Electronics and Drive Systems. He is an Associate Editor for the IEEE TRANSACTIONS ON CIRCUITS AND SYSTEMS—II: EXPRESS BRIEFS and the *IET Renewable Power Generation*.

Li Li received the B.S. degree from the Huazhong University of Science and Technology, Wuhan, China, in 1996, the M.S. degree from Tsinghua University, Beijing, China, in 1999, and the Ph.D. degree from the University of California at Los Angeles, Los Angeles, CA, USA, in 2005, all in electrical engineering.

From 2005 to 2007, he was a Research Associate with the University of New South Wales, Australian Defence Force Academy (UNSWADFA), Canberra, ACT, Australia. From 2007 to 2011, he was a Researcher with National ICT Australia, Victoria Research Laboratory, Department of Electrical and Electronic Engineering, The University of Melbourne, Melbourne, VIC, Australia. He held several visiting positions at the Beijing Institute of Technology, Beijing, Tsinghua University, and UNSWADFA. In 2011, he joined the University of Technology Sydney, Ultimo, NSW, Australia, where he is currently a Senior Lecturer. His current research interests include control theory and power system control.

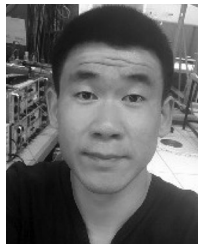

Jianwei Zhang (S'15) was born in Bayannur, China. He received the bachelor's degree in electrical engineering from Northwest A&F University, Yangling, China, in 2014. Since then, he has been working toward the Ph.D. degree in electrical engineering with the University of Technology Sydney, Sydney, NSW, Australia.

His research interests include control of power electronic converters, matrix converters, microgrids, and ac motor drives.

Linfeng Zheng (S'14) received the B.E. and M.E. degrees in electrical engineering from Beijing Jiaotong University, Beijing, China, in 2011 and 2014, respectively. He is currently working toward the Ph.D. degree with the University of Technology Sydney, Sydney, NSW, Australia.

His research interests include the development of battery and supercapacitor management and packaging techniques for electric vehicles and energy storage systems.

Jianguo Zhu (S'93–M'96–SM'03) received the B.E. degree from the Jiangsu Institute of Technology, Zhenjiang, China, in 1982, the M.E. degree from the Shanghai University of Technology, Shanghai, China, in 1987, and the Ph.D. degree from the University of Technology, Sydney (UTS), Sydney, NSW, Australia, in 1995, all in electrical engineering.

He is currently a Professor at the School of Electrical and Data Engineering, UTS. His current research interests include electromagnetics, magnetic properties of materials, electrical machines and drives, power electronics, and green energy systems.